Available online at www.sciencedirect.com
ScienceDirect
Geochimica et Cosmochimica Acta 75 (2011) 5496–5509
Geochimica et Cosmochimica Acta
www.elsevier.com/locate/gca

An experimental study of crystalline basalt dissolution from $2 \leqslant pH \leqslant 11$ and temperatures from 5 to 75 °C

Snorri Gudbrandsson [a,b,*], Domenik Wolff-Boenisch [a], Sigurdur R. Gislason [a], Eric H. Oelkers [b]

[a] Institute of Earth Sciences, University of Iceland, Sturlugata 7, 101 Reykjavik, Iceland
[b] GET, CNRS/UMR 5563-Université Paul Sabatier, 14 rue Edouard Belin, 31400 Toulouse, France

Received 2 December 2010; accepted in revised form 22 June 2011; available online 1 July 2011

Abstract

Steady-state element release rates from crystalline basalt dissolution at far-from-equilibrium were measured at pH from 2 to 11 and temperatures from 5 to 75 °C in mixed-flow reactors. Steady-state Si and Ca release rates exhibit a U-shaped variation with pH where rates decrease with increasing pH at acid condition but increase with increasing pH at alkaline conditions. Silicon release rates from crystalline basalt are comparable to Si release rates from basaltic glass of the same chemical composition at low pH and temperatures $\geqslant 25$ °C but slower at alkaline pH and temperatures $\geqslant 50$ °C. In contrast, Mg and Fe release rates decrease continuously with increasing pH at all temperatures. This behaviour is interpreted to stem from the contrasting dissolution behaviours of the three major minerals comprising the basalt: plagioclase, pyroxene, and olivine. Calcium is primarily present in plagioclase, which exhibits a U-shaped dissolution rate dependence on pH. In contrast, Mg and Fe are contained in pyroxene and olivine, minerals whose dissolution rates decrease monotonically with pH. As a result, crystalline basalt preferentially releases Mg and Fe relative to Ca at acidic conditions. The injection of acidic CO_2-charged fluids into crystalline basaltic terrain may, therefore, favour the formation of Mg and Fe carbonates rather than calcite. Element release rates estimated from the sum of the volume fraction normalized dissolution rates of plagioclase, pyroxene, and olivine are within one order of magnitude of those measured in this study.

1. INTRODUCTION

A large number of studies have been performed to determine the dissolution rates of individual minerals in the laboratory as a function of temperature and reactive fluid composition (e.g. Lasaga et al., 1994; Brantley and Chen, 1995; Oelkers and Schott, 1995, 2001; Schott et al., 2009). Natural rocks, however, consist of a number of different minerals and glasses, each with distinct reactivities and surface areas. Geochemical modelling codes such as PHREEQC (Parkhurst and Appelo, 1999) sums together the dissolution rates of each mineral in a rock to estimate overall rock dissolution rates. This study aims to validate this geochemical modelling approach through experimental measurement of crystalline basalt dissolution. The present communication presents the results of these experiments and uses them to assess the application of individual mineral dissolution rates to describe those of a multi-phase rock.

Crystalline basalt was chosen for this study for a number of reasons. First, the selected basalt has a simple mineralogy, consisting mostly of olivine, pyroxene, and plagioclase. The dissolution rates of these minerals have been studied extensively over the past two decades (e.g. Chou and Wollast, 1985; Blum and Lasaga, 1991; Blum and Stillings, 1995; Oelkers and Schott, 1995; Stillings and Brantley, 1995; Pokrovsky and Schott, 2000b; Hänchen et al., 2006). Secondly, the composition of basalt can range from 100% glass to 100% crystalline. Experimentally measured basaltic glass

* Corresponding author at: GET, CNRS/UMR 5563-Université Paul Sabatier, 14 rue Edouard, Belin 31400 Toulouse Country, France. Tel.: +33 5 61 33 25 75; fax: +33 5 61 33 25 60.
E-mail address: snorgud@hi.is (S. Gudbrandsson).

0016-7037/$ - see front matter © 2011 Published by Elsevier Ltd.
doi:10.1016/j.gca.2011.06.035

dissolution rates have been reported in the literature (e.g. Oelkers and Gislason, 2001; Gislason and Oelkers, 2003; Wolff-Boenisch et al., 2004a,b, 2006; Flaathen et al., 2010; Stockmann et al., 2011). This study which investigates the reactivity of a basalt that contains 100% crystalline minerals allows direct assessment of the role of crystallinity on rates. Thirdly, a number of studies have considered the possibility of carbon storage in basaltic rocks (Dessert et al., 2003; McGrail et al., 2006; Marini, 2007; Matter et al., 2007; Goldberg et al., 2008; Kelemen and Matter, 2008; Oelkers et al., 2008; Prigiobbe et al., 2009b; Gislason et al., 2010). This process involves dissolution of basalt releasing divalent metal cations such as Ca^{2+}, Mg^{2+}, and Fe^{2+} to solution. These ions can react with dissolved CO_2 and precipitate as carbonate minerals. The rate limiting step for this reaction is commonly assumed to be the release of divalent cations from basalts (e.g. Marini, 2007; Oelkers et al., 2008). Knowledge of basalt dissolution rates is, therefore, paramount to assessing the efficiency of this potential carbon sequestration method. Fourthly, despite the large number of past studies on basalt dissolution coupled to secondary mineral precipitation (Gislason and Eugster, 1987a,b; Gislason et al., 1993; Navarre-Sitchler and Brantley, 2007; Wu et al., 2007; Gudbrandsson et al., 2008; Hausrath et al., 2009; Schaef and McGrail, 2009) few studies have investigated basalt dissolution in the dilute aqueous solutions relevant to continental surface weathering processes. Fifthly, because of its high reactivity, chemical weathering of basalt plays a significant role in the global cycle of numerous elements (Gislason et al., 1996, 2006, 2009; Brady and Gislason, 1997; Louvat and Allegre, 1997; Moulton et al., 2000; Dessert et al., 2001; Stefansson and Gíslason, 2001; Neaman et al., 2005; Eirikdsdottir et al., 2008; Hartmann et al., 2009; Allegre et al., 2010) and may play a significant role in the weathering of the Martian surface (e.g. Hausrath et al., 2008, 2009).

2. THEORETICAL BACKGROUND

The standard state adopted in this study is that of unit activity of pure minerals and H_2O at any temperature and pressure. For aqueous species other than H_2O, the standard state is unit activity of species in a hypothetical 1 m solution referenced to infinite dilution at any temperature and pressure. All thermodynamic calculations reported in this study were performed using the PHREEQC computer code (Parkhurst and Appelo, 1999) together with its phreeqc.dat database to which thermodynamic data have been added for magnesite, siderite, thomsonite, scolecite, mesolite, laumontite, heulandite, analcime, Ca-stilbite, Ca-mordenite, Ca-clinoptilolite, Fe-celadonite, antigorite, amorphous SiO_2, amorphous FeOOH, amorphous $Al(OH)_3$, gibbsite, allophane, and imogolite taken from Gysi and Stefansson (2011).

The crystalline basalt dissolved in this study is comprised of three major mineral phases, the pyroxene augite, the plagioclase labradorite, and a forsteritic olivine in addition to minor amounts of iron oxides. Pyroxene dissolution rates and mechanisms have been reported by Knauss et al. (1993), Brantley and Chen (1995), Oelkers and Schott (2001), Golubev et al. (2005), Dixit and Carroll (2007), and Daval et al. (2010). Pyroxene dissolution rates decrease continuously with increasing pH and are mildly inhibited by increasing divalent metal cation concentration. Oelkers (2001b) suggested that far-from-equilibrium pyroxene dissolution rates ($r_{+,py}$) can be described using

$$r_{+,py} = k_{py}\left(a_{H^+}^2 / a_{M^{2+}}\right)^{n_{py}} \quad (1)$$

where k_{py} designates a rate constant, a_i corresponds to the activity of the subscripted aqueous species, M^{2+} refers to the divalent metal present in the pyroxene and n_{py} stands for a stoichiometric coefficient equal to 1/8. A large number of studies have provided forsterite dissolution rates (e.g. Grandstaff, 1977; Kuo and Kirkpatrick, 1985; de Leeuw et al., 2000; Pokrovsky and Schott, 2000a,b; Rosso and Rimstidt, 2000; Oelkers, 2001a; Morales and Herbert, 2002; Olsen and Rimstidt, 2008; Prigiobbe et al., 2009a; Wimpenny et al., 2010). An equation describing far-from-equilibrium forsterite dissolution rates ($r_{+,fo}$) as a function of pH and solution composition is given by Pokrovsky and Schott (2000b)

$$r_{+,fo} = k_{Si,fo} \cdot \frac{K_{ads}^* \times a_{H^+}^{0.5}}{\left(1 + K_{ads}^* \times a_{H^+}^{0.5} + \frac{a_{Mg^{2+}}^2}{K_{ex} + a_{H^+}^4}\right)} + k_{Mg,fo} \quad \{> MgOH_2^+\} \quad (2)$$

where $k_{Si,fo}$ and $k_{Mg,fo}$ correspond to rate constants, K_{ads}^* and K_{ex} refer to equilibrium constants, and $\{> MgOH_2^+\}$ stands for the concentration of the $MgOH_2^+$ surface species. Most studies of plagioclase dissolution rates have focused on the dissolution rates of the albite end member (e.g. Chou and Wollast, 1984, 1985; Blum and Lasaga, 1991; Stillings and Brantley, 1995). Fewer studies have measured the dissolution rates of more Ca/Al-rich plagioclases (Oxburgh et al., 1994) and anorthite (Oelkers and Schott, 1995). Albite dissolution rates exhibit a synclinal form, where rates decrease with increasing pH at acidic conditions but increase with increasing pH at alkaline conditions. The far-from-equilibrium dissolution rates of An $\leqslant$ 80 plagioclases ($r_{+,plag}$) can be described using (Oelkers and Schott, 1995; Oelkers, 2001b)

$$r_{+,plag} = k_{plag}\left[\left(a_{H^+}^{3n_{plag}} / a_{Al^{3+}}^{n_{plag}}\right) K_T \Big/ \left(1 + K_T\left(a_{H^+}^{3n_{plag}} / a_{Al^{3+}}^{n_{plag}}\right)\right)\right] \quad (3)$$

where k_{plag} refers to a rate constant, n_{plag} is the stoichiometry coefficient equal to 1/3, and K_T stands for an equilibrium constant. This rate behaviour is similar to that of basaltic glass (Oelkers and Gislason, 2001) and other more acidic volcanic glasses (Wolff-Boenisch et al., 2004b). Note that a large body of experimental evidence indicates that n_{py} and n_{plag} in Eqs. (1) and (3) are temperature independent from at least $25 < T < 200$ °C (Oelkers and Schott, 2001; Oelkers, 2001b; Schott et al., 2009). The variation of the rate constants in Eqs. (1)–(3) with temperature can be estimated using the Arrhenius equation given by

$$K_i = A_A \exp(-E_A / RT) \quad (4a)$$

where E_A designates an activation energy, A_A denotes a pre-exponential factor, R stands for the gas constant, and T represents absolute temperature in K. Similarly, in the

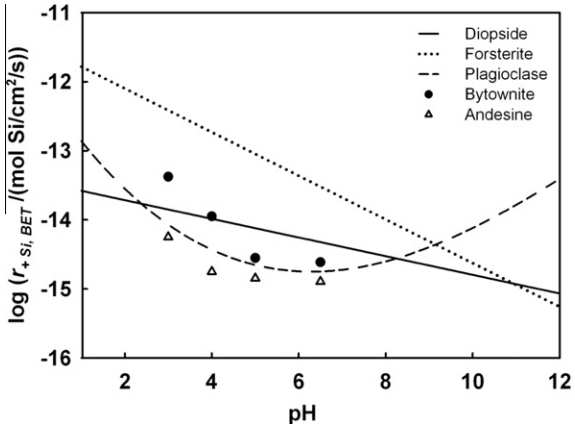

Fig. 1. Si release rates of selected minerals at 25 °C as a function of pH. The bytownite, andesine, forsterite, and diopside elemental rates illustrated in this figure were taken from Oxburgh et al. (1994), Pokrovsky and Schott (2000b), and Knauss et al. (1993), respectively. The plagioclase curve was obtained by multiplying the albite dissolution curve from Chou and Wollast (1985) by 4 to fit the bytownite and andesine rate data. This plagioclase curve was used to represent labradorite dissolution behaviour in this study.

absence of a mechanistic interpretation, apparent activation energies can be generated from measured dissolution rates using

$$r_i = A'_A \exp(-E'_A/RT) \quad (4b)$$

where E'_A designates an apparent activation energy, A'_A denotes a pre-exponential factor.

A comparison of the specific, far-from-equilibrium dissolution rates of diopside, forsterite, and plagioclase normalized to Si is shown as a function of pH at 25 °C in Fig. 1. The data sets chosen for this figure were those that covered the complete range of pH considered in this study. For example, diopside dissolution rates were chosen rather than those of augite to represent the rates of pyroxene dissolution as they are available for the full range of pH considered in this study. The plagioclase rate curve in this figure was obtained by adopting the albite dissolution curve from Chou and Wollast (1985) and fitting it to the measured dissolution rates for andesine (An_{46}) and bytownite (An_{76}) reported by Oxburgh et al. (1994). This dissolution rate curve was used in this study rather than previously published rate curves for plagioclase (e.g. Palandri and Kharaka, 2004) because these previous curves do not provide a description of the dissolution rates of the intermediate feldspars at alkaline conditions. Plagioclase dissolution rates are slower than those of diopside at pH 4–6 and forsterite at pH < 9. This is in concert with studies of weathering susceptibility of basaltic minerals and glass in soils at mildly acid to neutral pH (Crovisier et al., 1992; Gislason et al., 1996); basalt alteration was reported to proceed in the order olivine > pyroxene > plagioclase > sanidine according to Craig and Loughnan (1964), in the order glass > olivine > pyroxene > amphibole > plagioclase > pyroxene > opaque minerals according to Eggleton et al. (1987), and in the order glass, olivine > laihunite > clinopyroxene > orthopyroxene > plagioclase > K-feldspar according to Banfield et al. (1991). Similarly, the alteration of tertiary basalts in Iceland is first characterized by the hydrolysis of olivine and basaltic glass to form mixed-layer chlorite/smectite (Neuhoff, 1999). The latter stage of alteration is dominated by higher pH solutions and the replacement of plagioclase by zeolites and albite at high temperature (Neuhoff, 1999; Fridriksson et al., 2001). In contrast, Nesbitt and Wilson (1992) suggested this alteration order is olivine > glass > plagioclase > clinopyroxene > Fe–Ti-oxides. Taken together, these observations suggest that at acidic to neutral pH crystalline basalt dissolution will exhibit the preferential release of those elements that are present in olivine and pyroxene, such as Mg and Fe, whereas at basic pH crystalline basalt dissolution will release preferentially elements present in plagioclase, such as Ca and Al. The degree to which this is the case can be assessed by the experiments described below.

3. MATERIALS AND METHODS

Crystalline basalt was collected from a basaltic dyke on Stapafell Mountain, SW-Iceland. The sampled dyke had no

Table 1
Composition of crystalline and glassy basalt from the Stapafell Mountain, obtained by XRF analysis.

Sample	SiO_2	Al_2O_3	Fe_2O_3[b]	MgO	CaO	Na_2O	K_2O	TiO_2	MnO	P_2O_5	LOI	Total
Crystalline	47.9	13.4	12.3	10.0	12.2	1.5	0.3	1.6	0.2	0.2	−0.5	99.1
Glass[a]	48.1	14.6	10.9	9.1	11.8	2.0	0.3	1.6	0.2	0.2		98.8

[a] From Oelkers and Gislason (2001).
[b] Most iron in the +2 form (Oelkers and Gislason, 2001).

Table 2
Average composition of the major minerals present in the Stapafell crystalline basalt, determined with electron microprobe and reported as weight percentage of oxides.

Sample	#	SiO_2	TiO_2	Al_2O_3	FeO	MnO	MgO	CaO	Na_2O	K_2O	Total
Plagioclase	46	52.10	0.00	28.36	1.68	0.00	0.71	13.57	3.74	0.13	100.28
Olivine	8	39.74	0.03	0.07	15.53	0.21	45.00	0.37	0.01	0.00	100.95
Pyroxene	44	47.74	2.13	5.64	12.10	0.26	12.94	18.85	0.32	0.00	99.97

[#]Number of analyses.

visible alteration features. The composition of the sampled crystalline basaltic rock is similar to that of mid-ocean ridge basalts (MORB). This basalt was also chosen because dissolution rates for basaltic glass obtained from this site have been previously reported (Oelkers and Gislason, 2001; Gislason and Oelkers, 2003).

The bulk chemical composition of the sampled crystalline basalt was analyzed using a Panalytical PW2404 wavelength-dispersive sequential X-ray fluorescence spectrometer located at the University of Edinburgh. The measured composition is reported in Table 1 and is consistent with Si_1 $Ti_{0.025}$ $Al_{0.329}$ $Mg_{0.310}$ $Fe(III)_{0.02}$ $Fe(II)_{0.193}$ $Ca_{0.273}$ $Na_{0.061}$ $K_{0.007}$ $O_{3.394}$. This composition is nearly identical to that of Stapafell basaltic glass (Oelkers and Gislason, 2001; Gislason and Oelkers, 2003). The mineralogical composition of the basalt was determined by point counting. Four hundred points were counted from thin sections of the basalt; this analysis shows the basalt to contain 41.3 vol.% plagioclase (plag), 34.0 vol.% pyroxene (py), 15.8 vol.% olivine (ol), 4.7 vol.% iron oxides, and 4.2 vol.% glass. Such glass is likely Na and Si-rich compared to the bulk rock (Meyer and Sigurdsson, 1978). The volcanic glass was found in the samples collected close to the edge of the dyke, so experiments were performed on samples collected from the dyke centres. No volcanic glass was observed in the samples dissolved in this study by scanning electron microscope (SEM) imaging. The mineral composition of the basalt was also determined using a Stoe Stadi P Transmission XRD. Scans were run from 5° to 109.99° with a 0.05° step. Mineral abundance was determined by XRD peak intensity. This analysis suggests that the relative volume proportion of plag:py:ol is 44:39:17.

The chemical composition of the minerals in the crystalline basalt was determined from standard wavelength dispersive techniques using a JEOL Superprobe JSL 8200 located at the University of Copenhagen. These analyses were performed using an acceleration voltage of 15 kV, a

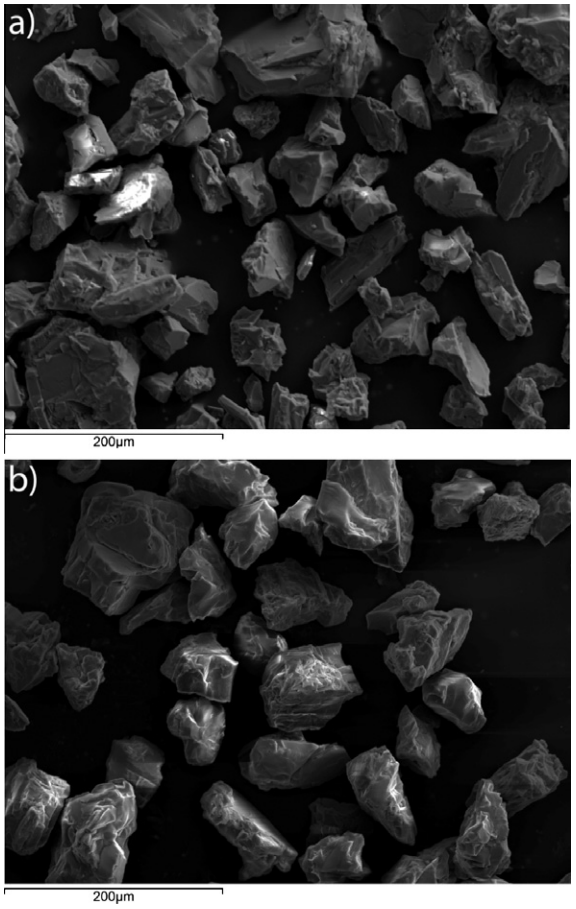

Fig. 3. SEM photomicrographs of the crystalline basalt. (a) The crystalline basalt before dissolution experiments, (b) the basalt after it was dissolved in dissolution experiments at pH 10 at 25, 50, and 75 °C for total of 623 h. No secondary phases are observed and the edges seem to be somewhat rounded by the dissolution.

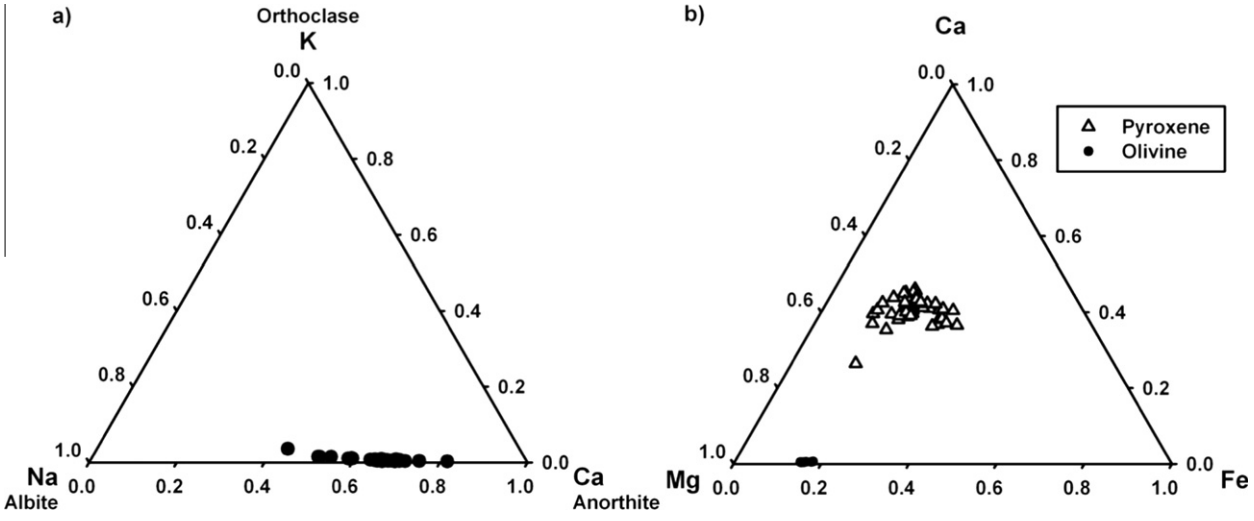

Fig. 2. Mineralogical compositions of the minerals in the basalt used in presented study plotted in ternary diagram. (a) The compositions of 46 analyzed plagioclase grains, (b) the compositions of 44 analyzed pyroxene and 8 analyzed olivine grains. Chemical analyses were performed by microprobe.

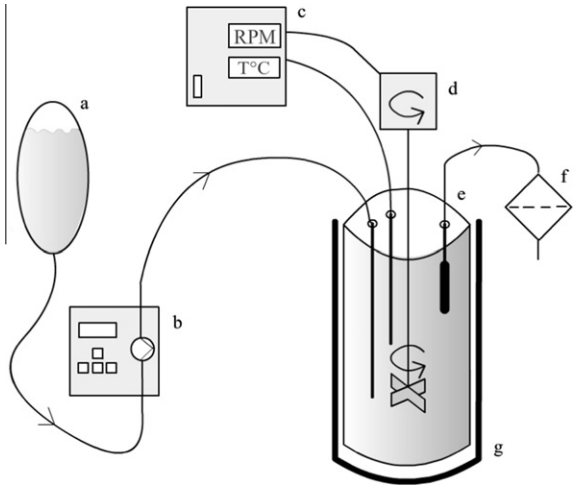

Fig. 4. Experimental design: (a) inlet solution container, (b) high pressure liquid chromatography (HPLC) pump, (c) temperature and rotation speed control, (d) stirring motor, (e) 300 mL Ti-reactor from Parr™ Instrument equipped with, from left, fluid inlet tube, thermocouple, magnetic stirrer, and fluid outlet fixed with a 2 μm Ti filter, (f) outlet solution goes through 0.2 μm cellulose acetate filter before sampling and ICP analysis, (g) thermal insulation and furnace.

beam current of 15 nA and a beam diameter of 2 μm. Natural and synthetic minerals and glasses were used as standards to check for potential drift. The resulting mineralogical composition of the basalt is given in Table 2 and is displayed graphically in Fig. 2. In total, 98 grains were analyzed, 46 plagioclase, 8 olivine, and 44 pyroxene. The microprobe data show that the plagioclase is of labradoritic composition (An_{65}), the olivine has a forsterite component of Fo_{85} and the pyroxene is of augite composition. The measured density of the crystalline basalt is 3.03 g/cm^3, in agreement with a calculated density of 3.11 g/cm^3 using the density of each mineral and its volume in the crystalline basalt.

The crystalline basalt was dried at room temperature for several days before it was ground using a jaw crusher. The finely grained material was dry sieved to obtain the 45–125 μm size fraction. This size fraction was subjected to gravitational settling to remove ultra-fine particles and subsequently cleaned ultrasonically five times in deionized water and then in acetone. The resulting powder was oven-dried at 50 °C for several days. An SEM image of the resulting crystalline basalt powder is shown in Fig. 3. The surfaces are free of fine particles. Most individual grains consist of single minerals, although some multi-mineral grains are evident. The specific surface area of the cleaned and dried 45–125 μm size fraction was determined to be 7030 cm^2/g via 11 point krypton adsorption using a Quantachrome Gas Sorption system. The geometric surface area of the powder was calculated using $A_{geo} = 6/(\rho * d_{eff})$ (Tester et al., 1994) where ρ designates the particle density (3.03 g/cm^3) and d_{eff} represents the effective particle diameter. The number 6 is based on the assumption that grains have a smooth spherical shape. This calculation yields a geometric surface area of 246 cm^2/g. The ratio between BET and geometric surface area (A_{BET}/A_{geo}) is the roughness factor, which equals 28.6.

Table 3
Initial conditions and inlet solution compositions for all experiments.

Experiment No.	Experiments series	pH	HCl (mmol/kg)	NH_4OH (mmol/kg)	NH_4Cl (mmol/kg)	Mass of basalt (g)
02-05	A	2	33.46	0	0	4.02
03-05	A	3	3.35	0	8.97	4.02
03-25	B	3	3.35	0	8.97	2.07
03-50	C	3	3.35	0	8.97	3.30
04-05	A	4	0.33	0	9.91	4.02
04-25	D	4	0.33	0	9.91	3.99
04-50	D	4	0.33	0	9.91	3.99
04-75	D	4	0.33	0	9.91	3.99
05-05	E	5	0.03	0	9.91	5.19
05-25	E	5	0.03	0	9.91	5.19
05-50	E	5	0.03	0	9.91	5.19
05-75	E	5	0.03	0	9.91	5.19
06-25	F	6	0	0	9.91	6.00
07-50	F	7	0	0	9.91	6.00
07-75	F	7	0	0	9.91	6.00
09-05	G	9	0	5.04	9.98	4.51
09-25	G	9	0	5.04	9.98	4.51
09-50	H	9	0	5.04	9.98	5.05
09-75	H	9	0	5.04	9.98	5.05
10-25	I	10	0	50.04	9.85	4.38
10-50	I	10	0	50.04	9.85	4.38
10-75	I	10	0	50.04	9.85	4.38
11-05	J	11	0	502.04	8.96	4.50
11-25	J	11	0	502.04	8.96	4.50
11-50	K	11	0	502.04	8.96	4.50
11-75	K	11	0	502.04	8.96	4.50

Crystalline basalt dissolution experiments were performed at pH from 2 to 11 in a Parr™ mixed flow reactor system, as illustrated in Fig. 4. This system consists of a 300 mL titanium reactor with external temperature and stirring controls. Reactive fluids were injected into this reactor via a high pressure liquid chromatography (HPLC) pump allowing a constant flow rate from 0.5 to 4.5 mL/min. The inlet fluids were made of deionized water and Merck analytical grade NH_4Cl, HCl, and NH_4OH and had an ionic strength of 0.01 mol/kg. The compositions of all inlet solutions used in this study are reported in Table 3. The inlet solutions with neutral and alkaline pH were initially bubbled with N_2 and then continuously kept under a N_2 atmosphere to prevent CO_2 dissolution into this fluid. The reactor was cleaned thoroughly, assembled, and run for at least 24 h with deionized water and then for another 24 h with the inlet solution to rinse the tubing and clean the reactor prior to each experiment. At the end of this cleaning cycle an outlet fluid sample was taken for chemical analysis.

Experiments were initiated by placing between 1 and 5 g of dry basalt powder into the reactor. The reactor was then filled with the inlet solution, sealed, and placed in a furnace jacket. Reactive fluid flow, temperature, and stirring rates were adjusted to desired settings. The fluid/basalt powder mixture was continuously stirred at approximately 400 rpm. Gislason and Oelkers (2003) observed that rotation speeds in excess of 325 rpm was sufficient to maintain surface reaction control of basaltic glass dissolution at pH 3.3. Outlet solutions were regularly sampled, filtered using 0.2 μm cellulose acetate filters, and then acidified with

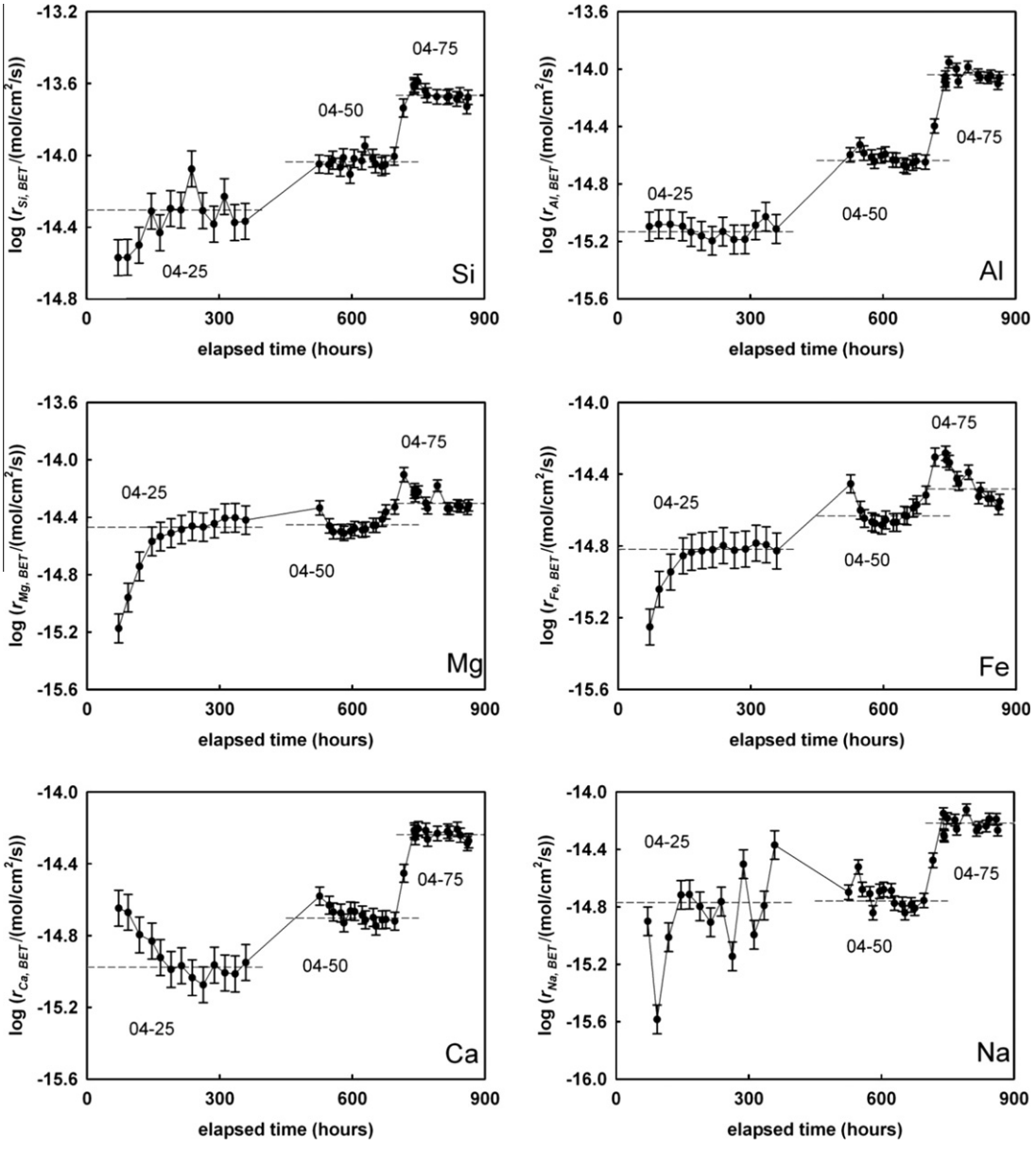

Fig. 5. Elemental release rates, $r_{i,\mathrm{BET}}$ during experiments performed at pH 4 and 25, 50, and 75 °C as part of a single experimental series. The symbols correspond to measured $r_{i,\mathrm{BET}}$ whereas the dashed lines correspond to their steady state values.

concentrated supra-pure HNO_3 prior to their analysis for Si, Mg, Na, Al, Fe, and Ca by ICP-OES. As was the case for a number of recent mineral dissolution rate studies (e.g. Flaathen et al., 2010; Saldi et al., 2010; Oelkers et al., 2011) experiments in this study were run in series. Each series consisted of a set of dissolution experiments performed on the same basalt powder. The experiments performed in each experimental series are listed in Table 3. Each experiment was run until a constant Si release rate was observed. Steady-state was confirmed by at least three consecutive outlet solution Si measurements performed on samples taken over a period of at least 10 residence times (the residence time is the ratio of the reactor volume to the fluid flow rate). This steady-state criterion was met for all experiments. After reaching constant Si release rates, temperature, flow rate or inlet fluid compositions were adjusted to new values and a new experiment began. Each experimental series was stopped before 5% of the initial basalt was dissolved.

4. RESULTS

Twenty six crystalline basalt dissolution experiments were performed in this study. The reactive fluid concentrations of Si, Al, Mg, Fe, Ca, and Na were regularly measured. These concentrations were used to calculate element release rates ($r_{i,j}$) using

$$r_{i,j} = \frac{C_i FR}{A_j m} \tag{5}$$

where c_i represents the concentration of the ith element in the outlet fluid, FR designates the fluid flow rate, A_j and m refer to the specific surface area and mass of the solid in the reactor, respectively. The surface area used throughout this study was obtained from BET analysis (A_{BET}). Each dissolution experiment was run until steady-state rates were attained. Steady-state Si and Al release rates were rapidly attained in all experiments as illustrated by the temporal evolution of $r_{i,BET}$ values of experimental series 04-25 to 04-75 shown in Fig. 5. This series included experiments at three distinct steady-state conditions at pH 4 and 25, 50, and 75 °C. Mg and Fe release rates appear to take longer to attain steady-state; this may be a consequence of divalent metal–proton exchange reactions occurring on the mineral surfaces (cf. Oelkers et al., 2009).

A summary of all measured steady-state $r_{Si,BET}$ is given in Table 4 and are shown as a function of pH in Fig. 6. These rates exhibit the characteristic dissolution behaviour exhibited by aluminosilicate minerals; rates decrease with increasing pH at acidic conditions and increase with increasing pH at basic conditions. The dashed curves in Fig. 6 correspond to $r_{Si,BET}$ from basaltic glass for a constant total dissolved Al concentration of 10^{-5} mol/kg as reported by Gislason and Oelkers (2003). The aqueous Al^{3+} activity is close to that of the experiments performed in this study. Rates measured in this study are compared to those for glass dissolution reported by Gislason and Oelkers (2003) because they were performed on glass samples collected from the same site, having the same chemical composition, age, and weathering history as the crystalline basalts

Table 4
Experimental results of Stapafell crystalline basalt dissolution experiments.

Experiment No.	Temperature (°C)	Samples[a] #	pH[b]	Flow rate[b] (g/min)	Run time (h)	C_{Si} (mol/kg × 10^{-6})	C_{al} (mol/kg × 10^{-6})	C_{ca} (mol/kg × 10^{-6})	C_{fe} (mol/kg × 10^{-6})	C_{mg} (mol/kg × 10^{-6})	log $r_{Si,BET}$ (mol/cm^2/s)
02-05	5	8	2.04	4.39	55.0	14.23	3.21	2.69	9.29	13.35	−13.44
03-05	5	8	3.05	2.71	155.0	4.11	0.85	1.49	2.71	4.03	−14.12
03-25	25	11	2.94	1.34	481.5	9.92	1.02	1.72	4.07	10.85	−13.77
03-50	50	9	3.16	3.13	166.0	82.30	5.40	6.87	37.75	88.63	−12.76
04-05	5	11	4.06	1.61	225.0	1.01	0.55	1.62	0.59	0.70	−15.02
04-25	25	13	4.13	1.26	359.0	6.15	1.02	1.70	1.86	3.96	−14.31
04-50	50	15	4.09	1.67	357.5	10.02	2.57	2.23	2.64	3.93	−14.03
04-75	75	13	4.04	4.46	146.5	8.43	3.40	2.21	1.42	1.99	−13.67
05-05	5	6	5.00	0.53	224.0	1.33	0.88	2.16	1.18	0.42	−15.50
05-25	25	5	5.03	0.53	252.5	3.02	0.38	1.47	0.90	1.13	−15.13
05-50	50	6	5.14	0.54	240.0	9.00	0.25	2.46	0.51	0.95	−14.76
05-75	75	5	5.65	0.52	411.5	29.05	4.05	8.17	0.25	1.68	−14.16
06-25	25	10	5.86	0.54	886.0	1.95	0.38	0.59	0.29	0.37	−15.45
07-50	50	6	6.89	0.54	261.0	6.09	0.69	1.41	0.10	0.31	−14.95
07-75	75	5	6.59	0.54	190.0	35.22	0.66	10.13	n.g.	1.20	−14.13
09-05	5	8	9.24	0.87	431.0	1.43	0.43	0.33	0.13	0.20	−15.26
09-25	25	5	9.22	0.84	190.0	2.78	0.81	0.57	0.19	0.37	−14.94
09-50	50	6	9.28	0.53	224.0	15.24	4.65	2.81	0.13	1.14	−14.48
09-75	75	9	9.27	0.51	397.0	37.27	11.21	9.55	0.14	5.50	−14.06
10-25	25	7	10.10	1.16	284.0	5.60	0.77	0.99	0.21	0.32	−14.39
10-50	50	6	10.12	2.65	201.0	11.45	0.67	1.44	0.41	0.92	−13.75
10-75	75	5	10.09	2.97	138.0	19.04	4.22	3.71	0.11	1.94	−13.53
11-05	5	4	10.74	1.94	75.0	6.39	0.59	9.77	0.01	0.12	−14.24
11-25	25	4	11.01	2.04	72.5	10.58	1.37	4.47	0.01	0.04	−13.95
11-50	50	4	10.76	2.20	75.0	12.85	3.41	1.61	0.01	0.39	−13.89
11-75	75	4	10.96	3.23	72.5	31.71	11.67	5.14	0.02	0.84	−13.27

[a] Number of measured rates.
[b] Average value of all measured samples.

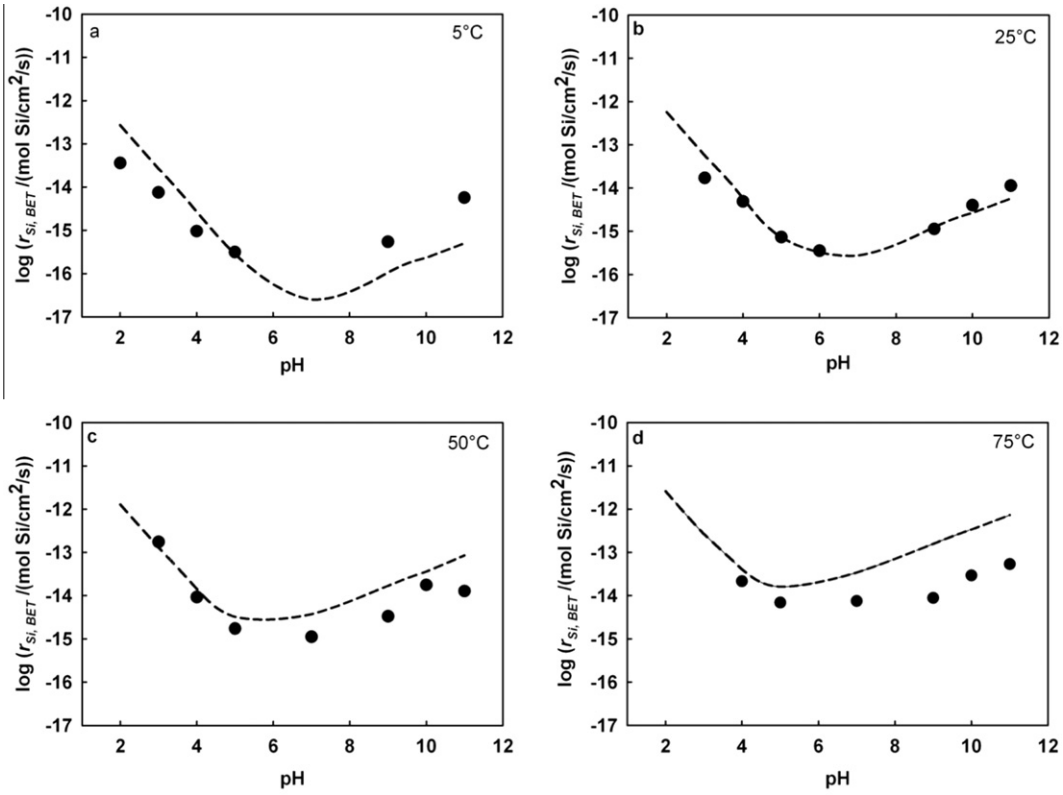

Fig. 6. Steady-state Si release rates versus pH at the indicated temperatures. The symbols correspond to measured $r_{Si,BET}$ from the crystalline basalt while the dashed curves represent $r_{Si,BET}$ from basaltic glass dissolution calculated using the equation reported by Gislason and Oelkers (2003) and an aqueous Al concentration of 10^{-5} mol/kg.

dissolved in this study. Measured $r_{Si,BET}$ for the crystalline basalts are in general equal to or lower than those of the corresponding glass. The only exception is the 5 °C experiments at high pH where crystalline basalt dissolution appears to be slightly faster than that of basaltic glass. The observation that crystalline basalt dissolution rates are in general slower than those of basaltic glass is consistent with the conclusions of Wolff-Boenisch et al. (2006).

The ratio of the release rate of each element relative to Si normalized to the corresponding ratio in the dissolving solid is displayed as a function of pH in Fig. 7. If this ratio is equal to one, the release rate of the element is stoichiometric relative to Si, if it is greater than one the element is preferentially released relative to Si, while if it is less than one the element is preferentially retained in the solid phase relative to Si. Mg and Fe tend to be preferentially released from the basalt at acid conditions and preferentially retained at higher pH. Ca is somewhat retained by the solid phase at low pH, but exhibits close to stoichiometric release relative to Si at circum neutral pH. With few exceptions, Al is retained by the solid phase at all temperatures and pH conditions considered in this study.

Steady-state outlet fluid compositions were used to calculate the saturation state of primary and potential secondary mineral phases in all experiments. The results of these calculations are shown in Annex A. The pH 3 outlet fluids were calculated to be undersaturated with respect to all primary and potential secondary minerals while the neutral to high pH outlet fluids were calculated to be supersaturated with respect to clinopyroxene, goethite, hematite, and gibbsite. Note however that the results shown in Annex A were calculated assuming the fluids were in equilibrium with atmospheric O_2, which is likely an overestimate of the oxygen content of these fluids which were purged with N_2 prior to their injection into the reactors. As such the saturation state of oxidized iron bearing minerals (e.g. hematite and goethite) is likely overestimated in these calculations. No secondary minerals were observed in the outlet filter or on the solids recovered following the experiments by SEM analysis suggesting that these oxidized iron minerals were in fact undersaturated in the reactive fluids.

5. DISCUSSION

5.1. Elemental release rates and CO_2 storage

The results in this study illustrate the contrasting dissolution behaviour of a multi-mineral silicate rock versus its corresponding glass. Si release from both crystalline and glassy basalt exhibits a similar pH dependency, though at basic pH Si appears to be released somewhat faster from glass at 5 °C but slower at 75 °C (Fig. 6). Furthermore, the Mg and Fe release rates decrease continuously with increasing pH (see Fig. 8) while those of Si and Ca display

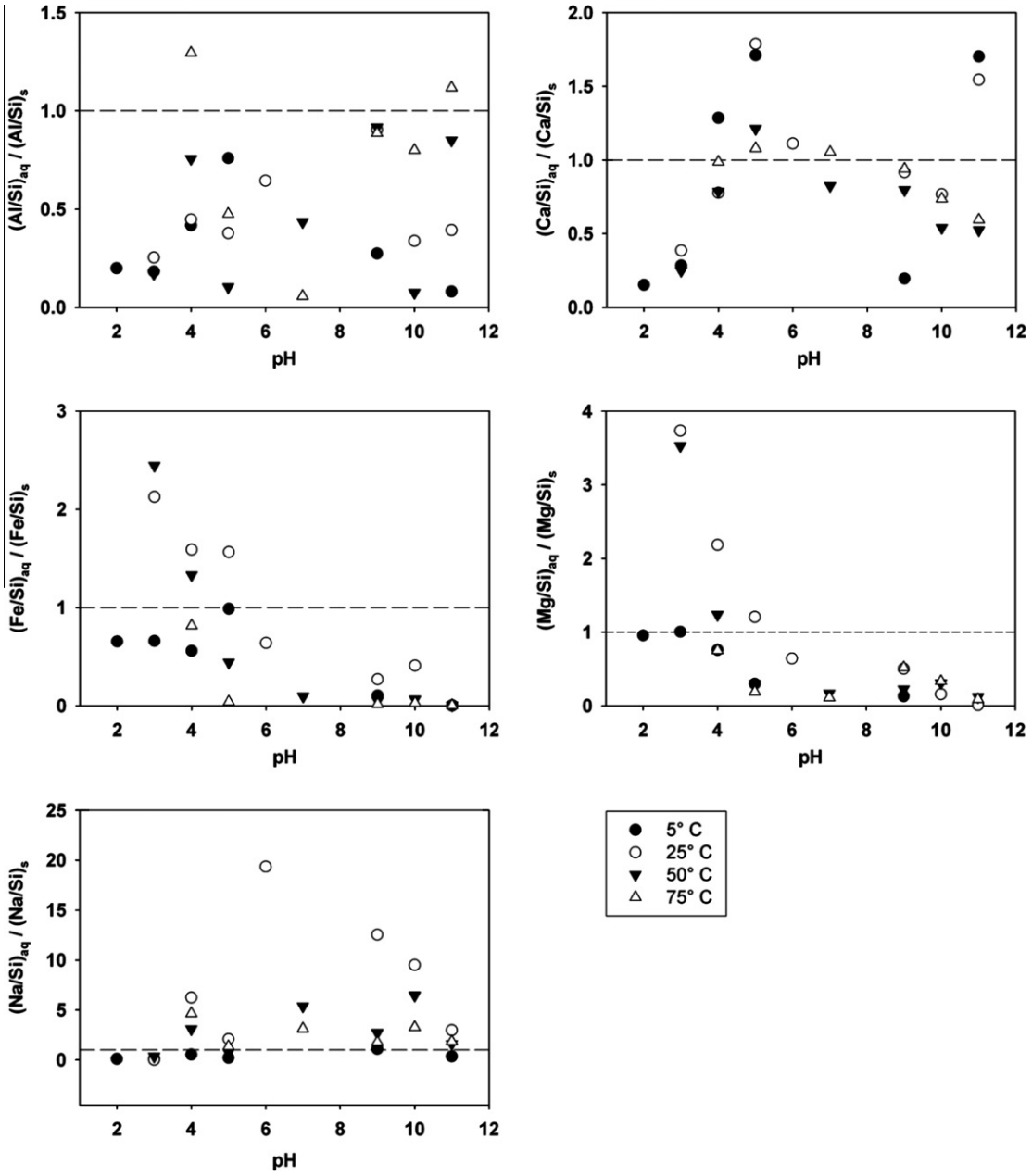

Fig. 7. The relative steady-state release of elements to aqueous solution divided by the corresponding element ratio of crystalline basalt plotted as a function of pH. Filled circles, open circles, filled triangles, and open triangles correspond to rates measured at 5, 25, 50, and 75 °C, respectively. The dashed line corresponds to stoichiometric release rates of the elements.

a synclinal shaped pH dependence. It seems likely that the distinct behaviour of crystalline basalt stems from the contrasting dissolution behaviours of its constituent minerals. The bulk of the Mg and Fe in the crystalline basalt are contained in olivine and pyroxene (see Table 2). In contrast to the dissolution behaviour of basaltic glass, the dissolution rates of olivine and pyroxene decrease monotonically with increasing pH (see Fig. 1). The effect of the distinct mineral dissolution behaviour also affects strongly the release rates of calcium. As can be deduced from Fig. 1, crystalline basalt dissolution at acid pH is dominated by the dissolution of olivine, which has a specific dissolution rate at least one order of magnitude higher than that of diopside and Ca-rich plagioclase. Olivine is Mg and Fe rich but Ca poor. As a result Ca tends to be retained by the solid at acid conditions.

The release of divalent metals to solution from silicates is an essential and perhaps rate-limiting step for the successful carbonatization of CO_2 during carbon storage efforts (cf. Oelkers et al., 2008; Schaef and McGrail, 2009; Gislason et al., 2010; Schaef et al., 2010). A significant observation presented above is that the relative

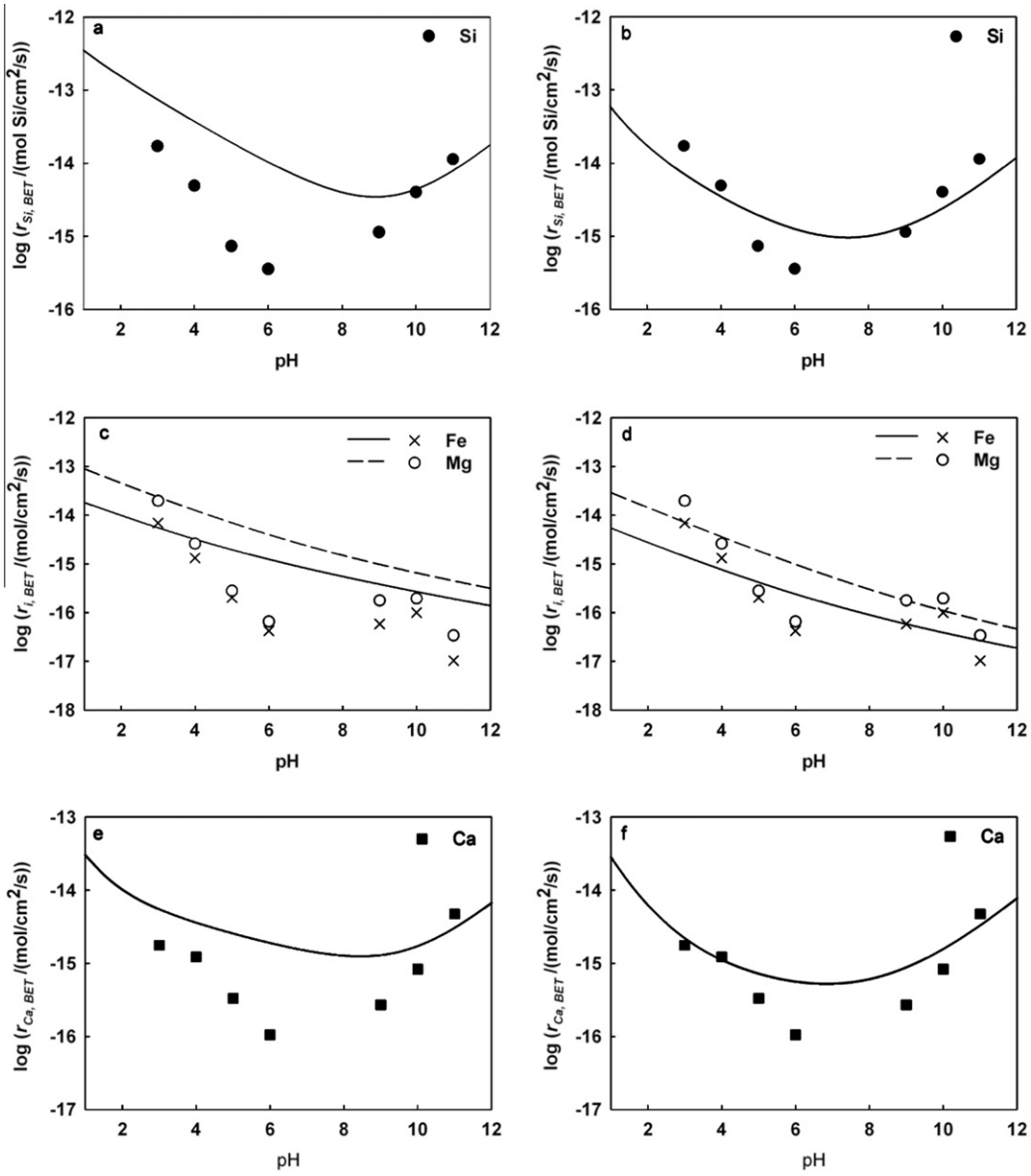

Fig. 8. Element release rates from dissolving crystalline basalts at 25 °C as a function of pH. The symbols correspond to measured release rates. The curves in plots a, c, and e represent $r_{i,BET}$ calculated assuming the reactive surface area of each mineral is proportional to its volume fraction, whereas the curves in plots (b, d, and f) stand for $r_{i,BET}$ calculated by fitting the reactive surface area of each mineral to the measured element release rates – see text for further clarification.

divalent metal release rates from crystalline basalts vary significantly with pH. The rate of Ca release from dissolving crystalline basalt as a fraction of the corresponding total divalent metal release rate at 25 °C is shown in Fig. 9. At pH 2–3 only 6–20% of the divalent metals released from basalt are calcium. At these conditions the divalent metal flux from crystalline basalt dissolution is dominated by Mg and Fe release. The fraction of Ca released increases continuously with rising pH. At pH 11, more than 80% of the divalent metal flux is Ca. Since CO_2 charged waters are acidic, crystalline basalt dissolution will release far more Mg and Fe than Ca to solution, favouring the formation of magnesite, siderite, and mixed Fe–Mg carbonates rather than calcite. This assumption is corroborated by observations of secondary carbonate formation during the alteration of basaltic lavas by CO_2-rich fluids in West Greenland (Rogers et al., 2006). Carbonates formed in this system in the initially CO_2-rich, low pH fluids are Fe and Mg-rich. Only late stage carbonates are Ca-rich. The degree to which such Mg-rich carbonates form in other systems, however, depends on their nucleation and growth rates, which may be sluggish, compared to that of calcite (Saldi et al., 2009).

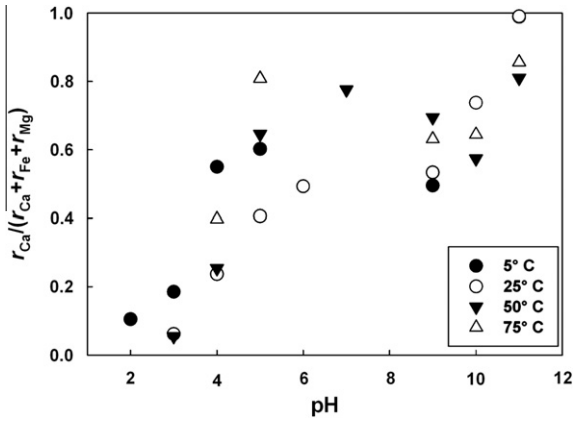

Fig. 9. Ca release rates divided by the sum of the release rates of the divalent cations from crystalline basalt at all pH and temperatures. Filled circles, open circles, filled triangle and open triangles correspond to rates measured at 5, 25, 50, and 75 °C, respectively.

5.2. Modelling element release rates from mineral dissolution rates

One of the great challenges in geochemistry is the successful prediction of chemical mass transfer rates during water–mineral interaction. Element release rates from the crystalline basalt dissolution experiments performed in this study are dominated by the dissolution of its three major minerals: olivine, pyroxene, and plagioclase. In the absence of secondary mineral precipitation and contributions from the dissolution of glass and minor minerals, the release rate of the ith element from crystalline basalt ($r_{i,j}$) can be approximated by

$$r_{i,j} = \sum_{k=0}^{N} \frac{A_{j,k}}{A_j} v_{i,k} r_{j,k} = \frac{A_{j,\mathrm{palg}}}{A_j} v_{i,\mathrm{plag}} r_{j,\mathrm{palg}} + \frac{A_{j,\mathrm{ol}}}{A_j} v_{i,\mathrm{ol}} r_{j,\mathrm{ol}} + \frac{A_{j,\mathrm{py}}}{A_j} v_{i,\mathrm{py}} r_{j,\mathrm{py}} \quad (6)$$

where $r_{j,k}$ refers to the dissolution rate of the kth mineral (plag, ol, py) normalized to the jth surface area, $v_{i,k}$ designates the stoichiometric number of the ith element in the kth mineral, $A_{j,k}$ symbolizes the jth specific surface area of the kth mineral and A_j is the overall surface area. Eq. (6) was used in the present study to model measured steady-state element release rates from crystalline basalt by adopting the 25 °C dissolution rates as a function of pH of olivine reported by Pokrovsky and Schott (2000b), those of diopside reported by Knauss et al. (1993), to correspond to that of augite, and those of plagioclase taken from Fig. 1. Stoichiometric coefficients in Eq. (6) were taken from the mineral compositions listed in Table 2. To the first approximation, it seems reasonable to assume that the relative surface area of the three minerals comprising the crystalline basalt is proportional to the relative volume percent of each mineral in the dissolving basalt (e.g. 17%, 39%, and 44% for ol, py, and plag, respectively). The results of this calculation are plotted as curves and compared with measured element release rates in Fig. 8a, c, and e. Although these calculations exhibit the correct rate trends with pH, calculated steady-state release rates are approximately one order of magnitude faster than (a) measured Si release rates at acid to neutral pH, (b) measured Mg and Fe release rates at all pH, and (c) measured Ca release rates at intermediate pH. It should be noted that the uncertainties in the rates adopted to perform this calculation are significant and include such factors as variable mineral compositions and the affect of reactive fluid composition other than pH on rates. Differences between measured and computed rates such that observed in Fig. 8a, c, and e, are therefore, likely within the margin of error in the calculations. It seems unlikely that the difference between the curves and data points in Fig. 8 stem from contributions from the dissolution of minor phases (e.g. interstitial glass) as measured rates are slower than those computed using Eq. (6).

Table 5
Apparent activation energies (E'_a) obtained from this study. # symbolizes the number of steady-state rates used in the regression for E'_a and R^2 stands for the correlation coefficient of a linear regression through these rates.

	E'_a (kJ/mol)	#	R^2
pH 3	54.1	3	0.93
pH 4	33.8	4	0.96
pH 5	35.2	4	0.98
pH 9	33.9	4	0.99
pH 10	35.0	3	0.95
pH 11	24.2	6	0.98

An improved fit of measured element release rates was obtained by adjusting the relative surface areas of the minerals to 2.8% olivine, 13.9% pyroxene, and 83.3% plagioclase. The results of this fit are compared to measured steady-state element release rates in Fig. 8b, d, and f. This revised fit reproduces the measured element release rates within 0.5 log units at all pH. There are several reasons why the relative surface area of the minerals of the best data fit do not match the relative volume fraction of the minerals. First, pyroxene may be close to equilibrium (see the calculated saturation state of various minerals at steady-state in Annex A); rates slow as fluids approach equilibrium with respect to dissolving mineral phases (cf. Schott and Oelkers, 1995). Secondly, the grinding of the crystalline basalt may have created reactive surfaces in a heterogeneous way among the mineral phases. This may lead to a higher relative surface area for plagioclase, which is commonly comprised of fine-grained exsolution lamellae.

Apparent activation energies of Si release from crystalline basalt dissolution calculations using Eq. (4b) and the rates listed in Table 4 are near to 30 kJ/mol at pH $\geqslant$ 4 but increase to 54 kJ/mol at pH 3 (see Table 5). These values are close to the activation energies reported in the literature for basaltic glass; Gislason and Oelkers (2003) reported an activation energy for basaltic glass dissolution of 25.5 kJ/mol and Wolff-Boenisch et al. (2004a) reported activation energies of 27 kJ/mol at pH 4 and 41 kJ/mol at pH 10.6.

6. CONCLUSIONS

The results described above illustrate the contrasting behaviour of crystalline basalt versus basaltic glass. Although steady-state $r_{\mathrm{Si,BET}}$ of crystalline basalts and basal-

tic glass exhibit similar pH dependencies the release rates of the divalent metal cations differ significantly. Because of the distinct dissolution behaviour of its constituent minerals, Mg and Fe are preferentially removed from crystalline basalt at acid conditions, whereas Ca is preferentially removed at basic conditions. These observations suggest contrasting alteration behaviours of glassy versus crystalline basalt both during carbon sequestration and natural processes.

Element release rates estimated from the sum volume fraction normalized dissolution rates of plagioclase, pyroxene, and olivine are within one order of magnitude of those measured in this study and reproduce the distinct behaviour of the major elements. The degree to which this is an acceptable approximation of the dissolution behaviour of a crystalline rock most certainly depends on the system and the required accuracy. The critical parameter of such estimates, $\frac{A_{j,k}}{A_j}$, the relative reactive surface area of each mineral that is in contact with the reactive fluid, is impossible to predict *a priori* at present. Thus, although element release rate estimates based on the assumption that reactive surface area of individual minerals is proportional to its volume fraction in a rock can only present a crude approximation, it may provide some insight into dissolution behaviour of multi-phase rocks.

ACKNOWLEDGMENTS

The authors thank our friends and colleagues, including Helgi A. Alfredsson, Gabrielle J. Stockmann, Alexander P. Gysi, Iwona Monika Galeczka, Mahnaz Rezvani Khalilabad, Kiflom Gebrehiwot, Eydís Salome Eiríksdóttir, Andri Stefánsson, and Niels Óskarsson at the University of Iceland, Hólmfríður Sigurðardóttir, Einar Gunnlaugsson, Ingvi Gunnarsson, Edda Sif Aradóttir, and Bergur Sigfússon at Reykjavík Energy, Ivan Sanchez, Caroline Hem, and Susan Stipp at the NanoGeo Center at the University of Copenhagen, and Alfons Berger at the University of Copenhagen: This study was funded by The Environmental Fund of Reykjavík Energy through the CARB-FIX project, the European Community through the MIN-GRO Research and Training Network (MRTN-CT-2006-035488) and Delta-Min (Mechanisms of Mineral Replacement Reactions; Grant PITN-GA-2008-215360) and the Nordic Mineralogy Network.

APPENDIX A. SUPPLEMENTARY DATA

Supplementary data associated with this article can be found, in the online version, at doi:10.1016/j.gca.2011.06.035.

REFERENCES

Allegre C. J., Louvat P., Gaillardet J., Maynadier L., Rad S. and Capmas F. (2010) The fundamental role of island arc weathering in the oceanic Sr isotope budget. *Earth Planet. Sci. Lett.* **292**, 51–56.

Banfield J. F., Jones B. F. and Veblen D. R. (1991) An AEM–TEM study of weathering and diagenesis, Abert Lake, Oregon. 1: Weathering reactions in the volcanics. *Geochim. Cosmochim. Acta* **55**, 2781–2793.

Blum A. E. and Lasaga A. C. (1991) The role of surface speciation in the dissolution of albite. *Geochim. Cosmochim. Acta* **55**, 2193–2201.

Blum A. E. and Stillings L. L. (1995) Feldspar dissolution kinetics. In *Chemical Weathering Rates of Silicate Minerals* (eds. A. F. White and S. L. Brantley). Mineralogical Society of America, Washington, DC.

Brady P. V. and Gislason S. R. (1997) Seafloor weathering controls on atmospheric CO_2 and global climate. *Geochim. Cosmochim. Acta* **61**, 965–973.

Brantley S. L. and Chen Y. (1995) Chemical weathering rates of pyroxenes and amphiboles. *Rev. Min.* **31**, 119–172.

Chou L. and Wollast R. (1984) Study of the weathering of albite at room-temperature and pressure with a fluidized-bed reactor. *Geochim. Cosmochim. Acta* **48**, 2205–2217.

Chou L. and Wollast R. (1985) Steady-state kinetics and dissolution mechanisms of albite. *Am. J. Sci.* **285**, 963–993.

Craig D. C. and Loughnan F. C. (1964) Chemical and mineralogical transformations accompanying the weathering of basic volcanic rocks from New South Wales. *Aust. J. Soil Res.* **2**, 218–234.

Crovisier J. L., Honnorez J., Fritz B. and Petit J. C. (1992) Dissolution of subglacial volcanic glasses from Iceland: laboratory study and modelling. *Appl. Geochem.* **7**, 55–81.

Daval D., Hellmann R., Corvisier J., Tisserand D., Martinez I. and Guyot F. (2010) Dissolution kinetics of diopside as a function of solution saturation state: macroscopic measurements and implications for modeling of geological storage of CO_2. *Geochim. Cosmochim. Acta* **74**, 2615–2633.

de Leeuw N. H., Parker S. C., Catlow C. R. A. and Price G. D. (2000) Modelling the effect of water on the surface structure and stability of forsterite. *Phys. Chem. Miner.* **27**, 332–341.

Dessert C., Dupré B., François L. M., Schott J., Gaillardet J., Chakrapani G. and Bajpai S. (2001) Erosion of Deccan Traps determined by river geochemistry. Impact on global climate and $^{87}Sr/^{86}Sr$ ratio of seawater. *Earth Planet. Sci. Lett.* **188**, 459–474.

Dessert C., Dupré B., Gaillardet J., François L. M. and Allegre C. J. (2003) Basalt weathering laws and the impact of basalt weathering on the global carbon cycle. *Earth Planet. Sci. Lett.* **188**, 459–474.

Dixit S. and Carroll S. A. (2007) Effect of solution saturation state and temperature on diopside dissolution. *Geochem. Trans.* **8**, 3.

Eggleton R. A., Foudoulis C. and Varkevisser D. (1987) Weathering of basalt – changes in rock chemistry and mineralogy. *Clays Clay Miner.* **35**, 161–169.

Eirikdsdottir E. S., Louvat P., Gislason S. R., Oskarsson N. and Hardottir J. (2008) Temporal variation of chemical and mechanical weathering in NE Iceland: evaluation of a steady-state model of erosion. *Earth Planet. Sci. Lett.* **272**, 78–88.

Flaathen T. K., Gislason S. R. and Oelkers E. H. (2010) The effect of aqueous sulphate on basaltic glass dissolution rates. *Chem. Geol.* **277**, 345–354.

Fridriksson T., Neuhoff P. S., Arnórsson S. and Bird D. K. (2001) Geological constraints on the thermodynamic properties of the stilbite–stellerite solid solution in low-grade metabasalts. *Geochim. Cosmochim. Acta* **65**, 3993–4008.

Gislason S. R., Arnorsson S. and Armannsson H. (1996) Chemical weathering in southwest Iceland: effects of runoff, age of rocks and vegetative/glacial cover. *Am. J. Sci.* **296**, 837–970.

Gislason S. R. and Eugster H. P. (1987a) Meteoric water–basalt interactions. 2: A field-study in NE Iceland. *Geochim. Cosmochim. Acta* **51**, 2841–2855.

Gislason S. R. and Eugster H. P. (1987b) Meteoric water–basalt interactions. 2: A laboratory study. *Geochim. Cosmochim. Acta* **51**, 2827–2840.

Gislason S. R. and Oelkers E. H. (2003) Mechanism, rates, and consequences of basaltic glass dissolution. II: An experimental

study of the dissolution rates of basaltic glass as a function of pH and temperature. *Geochim. Cosmochim. Acta* **67**, 3817–3832.

Gislason S. R., Oelkers E. H., Eiriksdottir E. S., Kardjilov M. I., Gisladottir G., Sigfusson G., Snorrason A., Elefsen S., Hardardottir J., Torssander P. and Oskarsson N. (2009) Direct evidence of the feedback between climate and weathering. *Earth Planet. Sci. Lett.* **277**, 213–222.

Gislason S. R., Oelkers E. H. and Snorrason Á. (2006) The role of river suspended material in the global carbon cycle. *Geology* **34**, 49–52.

Gislason S. R., Veblen D. R. and Livi K. J. T. (1993) Experimental meteoric water–basalt interactions – characterization and interpretation of alteration products. *Geochim. Cosmochim. Acta* **57**, 1459–1471.

Gislason S. R., Wolff-Boenisch D., Stefansson A., Oelkers E. H., Gunnlaugsson E., Sigurdardottir H., Sigfusson B., Broecker W. S., Matter J. M., Stute M., Axelsson G. and Fridriksson T. (2010) Mineral sequestration of carbon dioxide in basalt: a pre-injection overview of the carbfix project. *Int. J. Greenhouse Gas Control* **4**, 537–545.

Goldberg D. S., Takahashi T. and Slagle A. L. (2008) Carbon dioxide sequestration in deep-sea basalt. *Proc. Natl. Acad. Sci. USA* **105**, 9920–9925.

Golubev S. V., Pokrovsky O. S. and Schott Jaque (2005) Experimental determination of the effect of dissolved CO_2 on the dissolution kinetics of Mg and Ca silicates at 25 °C. *Chem. Geol.* **217**, 227–238.

Grandstaff D. E. (1977) Some kinetics of forsterite olivine dissolution. *Trans. Am. Geophys. Union* **58**, 539.

Gudbrandsson S., Wolff-Boenisch D., Gislason S. R. and Oelkers E. H. (2008) Dissolution rates of crystalline basalt at pH 4 and 10 and 25–75 °C. *Mineral. Mag.* **72**, 155–158.

Gysi A. P. and Stefansson A. (2011) CO_2–water–basalt interaction. II: Numerical simulation of low temperature CO_2 sequestration into basalts. *Geochim. Cosmochim. Acta*. doi:10.1016/j.gca.2011.05.037.

Hänchen M., Prigiobbe V., Storti G., Seward T. M. and Mazzotti M. (2006) Dissolution kinetics of fosteritic olivine at 90–150 °C including effects of the presence of CO_2. *Geochim. Cosmochim. Acta* **70**, 4403–4416.

Hartmann J., Jansen N., Durr H. H., Kempe S. and Kohler P. (2009) Global CO_2 consumption by chemical weathering: what is the contribution too highly active weathering regions? *Global Planet. Change* **69**, 185–194.

Hausrath E. M., Navarre-Sitchler A. K., Sak P., Steefel C. and Brantley S. L. (2008) Basalt weathering rates on Earth and the duration of liquid water on the plains of Gusev Crater, Mars. *Geology* **36**, 67–70.

Hausrath E. M., Neaman A. and Brantley S. L. (2009) Element release rates from dissolving basalt and granite with and without organic ligands. *Am. J. Sci.* **309**, 633–660.

Kelemen P. B. and Matter J. (2008) In situ carbonation of peridotite for CO_2 storage. *Proc. Natl. Acad. Sci. USA* **105**, 17295–17300.

Knauss K. G., Nguyen S. N. and Weed H. C. (1993) Diopside dissolution kinetics as a function of pH, CO_2, temperature, and time. *Geochim. Cosmochim. Acta* **57**, 285–294.

Kuo L. C. and Kirkpatrick R. J. (1985) Kinetics of crystal dissolution in the system diopside–forsterite–silica. *Am. J. Sci.* **285**, 51–90.

Lasaga A. C., Soler J. M., Ganor J., Burch T. E. and Nagy K. L. (1994) Chemical-weathering rate laws and global geochemical cycles. *Geochim. Cosmochim. Acta* **58**, 2361–2386.

Louvat P. and Allegre C. J. (1997) Present denumdation rates of the island of Reunion determined by river geochemistry: basalt weatehring and mass budget between chemical and mechanical erosions. *Geochim. Cosmochim. Acta* **61**, 3645–3669.

Marini L. (2007) Geological sequestration of carbon dioxide. In *Thermodynamics, Kinetics and Reaction Path Modeling*. Elsevier, Amsterdam, 470 pp.

Matter J. M., Takahashi T. and Goldberg D. (2007) Experimental evaluation of in situ CO_2–water–rock reactions during CO_2 injection in basaltic rocks: implications for geological CO_2 sequestration. *Geochem. Geophys. Geosyst.* **8**, 1–19.

McGrail B. P., Schaef H. T., Ho A. M., Chien Yi-J, Dooley J. J. and Davidson C. L. (2006) Potential for carbon dioxide sequestration in flood basalts. *JGR Res.* **111**, B12201. doi:10.1029/2005JB004169.

Meyer P. S. and Sigurdsson H. (1978) Interstitial acid glass and chlorophaeiti in Iceland. *Lithos* **11**, 231–241.

Morales T. A. and Herbert R. (2002) Surface chemistry and acidic dissolution of forsterite. *Geochim. Cosmochim. Acta* **66**, A521.

Moulton K. L., West J. and Berner R. A. (2000) Solute flux and mineral mass balance approaches to the quantification of plant effects on silicate weathering. *Am. J. Sci.* **300**, 539–570.

Navarre-Sitchler A. and Brantley S. (2007) Basalt weathering across scales. *Earth Planet. Sci. Lett.* **261**, 321–334.

Neaman A., Chorover J. and Brantley S. L. (2005) Implications of the evolution of organic acid moieties for basalt weathering over geological time. *Am. J. Sci.* **305**, 147–185.

Nesbitt H. W. and Wilson R. E. (1992) Recent chemical-weathering of basalts. *Am. J. Sci.* **292**, 740–777.

Neuhoff P. S. (1999) Thermodynamic properties and paragenesis of rock-forming zeolites. Ph.D. Dissertation, Standford University.

Oelkers E. H. (2001a) An experimental study of forsterite dissolution rates as a function of temperature and aqueous Mg and Si concentrations. *Chem. Geol.* **175**, 485–494.

Oelkers E. H. (2001b) General kinetic description of multioxide silicate mineral and glass dissolution. *Geochim. Cosmochim. Acta* **65**, 3703–3719.

Oelkers E. H. and Gislason S. R. (2001) The mechanism, rates and consequences of basaltic glass dissolution. I: An experimental study of the dissolution rates of basaltic glass as a function of aqueous Al, Si and oxalic acid concentration at 25 °C and pH = 3 and 11. *Geochim. Cosmochim. Acta* **65**, 3671–3681.

Oelkers E. H., Gislason S. R. and Matter J. (2008) Mineral carbonation of CO_2. *Elements* **4**, 333–337.

Oelkers E. H., Golubev S. V., Pokrovsky O. S. and Benezeth P. (2011) Do organic ligands affect calcite dissolutions rates? *Geochim. Cosmochim. Acta* **75**, 1799–1813.

Oelkers E. H., Golubev S. V., Chairat C., Pokrovsky O. S. and Schott J. (2009) The surface chemistry of multi-oxide silicates. *Geochim. Cosmochim. Acta* **73**, 4617–4634.

Oelkers E. H. and Schott J. (1995) Experimental study of anorthite dissolution and the relative mechanism of feldspar hydrolysis. *Geochim. Cosmochim. Acta* **59**, 5039–5053.

Oelkers E. H. and Schott J. (2001) An experimental study of enstatite dissolution rates as a function of pH, temperature, and aqueous Mg and Si concentration, and the mechanism of pyroxene/pyroxenoid dissolution. *Geochim. Cosmochim. Acta* **65**, 1219–1231.

Olsen A. A. and Rimstidt J. D. (2008) Oxalate-promoted forsterite dissolution at low pH. *Geochim. Cosmochim. Acta* **72**, 1758–1766.

Oxburgh R., Drever J. I. and Sun Y. T. (1994) Mechanism of plagioclase dissolution in acid-solution at 25 °C. *Geochim. Cosmochim. Acta* **58**, 661–669.

Parkhurst D. L. and Appelo C. A. J. (1999) User's guide to phreeqc (version 2) – a computer program for speciation, batch-

reaction, one-dimensional transport, and inverse geochemical calculations. U.S.G.S. Water Res. Inv. Report. 99-4259.

Palandri J. L. and Kharaka Y. K. (2004) A compilation of rate parameters of water-mineral interaction kinetics for application to geochemical modeling. U.S.G.S. Open file report 2004-1068, 64 p.

Pokrovsky O. S. and Schott J. (2000a) Forsterite surface composition in aqueous solutions: a combined potentiometric, electrokinetic, and spectroscopic approach. *Geochim. Cosmochim. Acta* **64**, 3299–3312.

Pokrovsky O. S. and Schott J. (2000b) Kinetics and mechanism of forsterite dissolution at 25 °C and pH from 1 to 12. *Geochim. Cosmochim. Acta* **64**, 3313–3325.

Prigiobbe V., Costa G., Baciocchi R., Hanchen M. and Mazzotti M. (2009a) The effect of CO_2 and salinity on olivine dissolution kinetics at 120 °C. *Chem. Eng. Sci.* **64**, 3510–3515.

Prigiobbe V., Hanchen M., Werner M., Baciocchi R. and Mazzotti M. (2009b) Mineral carbonation processes for CO_2 sequestration. *Greenhouse Gas Control Technol.* **9**, 4885–4890.

Rogers K. L., Neuhoff P. S., Pedersen A. K. and Bird D. K. (2006) CO_2 metasomatism in a basalt-hosted petroleum reservoir, Nuussuaq, West Greenland. *Lithos* **92**, 55–82.

Rosso J. J. and Rimstidt J. D. (2000) A high resolution study of forsterite dissolution rates. *Geochim. Cosmochim. Acta* **64**, 797–811.

Saldi G. D., Jordan G., Schott J. and Oelkers E. H. (2009) Magnesite growth rates as function of temperature and saturation state. *Geochim. Cosmochim. Acta* **73**, 5646–5657.

Saldi G. D., Schott J., Pokrovsky O. S. and Oelkers E. H. (2010) An experimental study of magnesite dissolution rates at neutral to alkaline conditions and 150 and 200 °C as a function of pH, total dissolved carbonate concentration and chemical affinity. *Geochim. Cosmochim. Acta* **74**, 6344–6356.

Schaef H. T. and McGrail B. P. (2009) Dissolution of Columbia River basalt under mildly acidic conditions as a function of temperature: experimental results relevant to the geological sequestration of carbon dioxide. *Appl. Geochem.* **24**, 980–987.

Schaef H. T., McGrail B. P. and Owen A. T. (2010) Carbonate mineralization of volcanic province basalts. *Int. J. Greenhouse Gas Control* **4**, 249–261.

Schott J. and Oelkers E. H. (1995) Dissolution and crystallization rates of silicate minerals as a function of chemical affinity. *Pure Appl. Chem.* **67**, 903–910.

Schott J., Pokrovsky O. S. and Oelkers E. H. (2009) The link between mineral dissolution/precipitation kinetics and solution chemistry. *Rev. Mineral. Geochem.* **70**, 207–258.

Stefansson A. and Gíslason S. R. (2001) Chemical weathering of basalts, Southwest Iceland: effect of rock crystallinity and secondary minerals on chemical fluxes to the ocean. *Am. J. Sci.* **301**, 513–556.

Stockmann G. J., Wolff-Boenisch D., Gislason S. R. and Oelkers E. H. (2011) Do carbonate precipitates affect dissolution kinetics? 1: Basaltic glass. *Chem. Geol.* **284**, 306–316.

Stillings L. L. and Brantley S. L. (1995) Feldspar dissolution at 25 °C and pH 3 – reaction stoichiometry and the effect of cations. *Geochim. Cosmochim. Acta* **59**, 1483–1496.

Tester J. W., Worley W. G., Robinson B. A., Grigsby C. O. and Feerer J. L. (1994) Correlating quartz dissolution kinetics in pure water from 25 to 625 °C. *Geochim. Cosmochim. Acta* **58**, 2407–2420.

Wimpenny J., Gislason S. R., James R. H., Gannoun A., Von Strandmann P. A. E. and Burton K. W. (2010) The behaviour of Li and Mg isotopes during primary phase dissolution and secondary mineral formation in basalt. *Geochim. Cosmochim. Acta* **74**, 5259–5279.

Wolff-Boenisch D., Gislason S. R., Oelkers E. H. and Putnis C. V. (2004a) The dissolution rates of natural glasses as a function of their composition at pH 4 and 10.6, and temperatures from 25 to 74 °C. *Geochim. Cosmochim. Acta* **68**, 4843–4858.

Wolff-Boenisch D., Gislason S. R. and Oelkers E. H. (2004b) The effect of fluoride on the dissolution rates of natural glasses at pH 4 and 25 °C. *Geochim. Cosmochim. Acta* **68**, 4571–4582.

Wolff-Boenisch D., Gislason S. R. and Oelkers E. H. (2006) The effect of crystallinity on dissolution rates and CO_2 consumption capacity of silicates. *Geochim. Cosmochim. Acta* **70**, 858–870.

Wu L. L., Jacobson A. D., Chan H. C. and Hausner M. (2007) Characterization of element release during microbe–basalt interaction at 28 °C. *Geochim. Cosmochim. Acta* **71**, 2224–2239.

Associate editor: Dimitri A. Sverjensky